Journal of the Brazilian Society of Mechanical Sciences and Engineering (2019) 41:323
https://doi.org/10.1007/s40430-019-1823-7

TECHNICAL PAPER

Multi-response optimization of electrochemical micromachining parameters for SS304 using polymer graphite electrode with $NaNO_3$ electrolyte based on TOPSIS technique

N. Pradeep[1] · K. Shanmuga Sundaram[1] · M. Pradeep Kumar[1]

Received: 9 February 2019 / Accepted: 5 July 2019 / Published online: 15 July 2019

Abstract
This research experimentally investigates the influence of electrochemical micromachining (ECMM) process parameters of SS304 alloy with "polymer graphite electrode (PGE)," employing sodium nitrate as the electrolyte solution. The machining parameters were considered based on their significance in machining such as machining voltage, duty cycle and electrolyte concentration to assess and evaluate their effect on response parameters such as material removal rate, over cut and taper angle. The experimental results revealed that 23 g/l of electrolyte concentration, machining voltage of 9 V and 55% duty cycle are considered as the optimal parameters for accessing the multi-response characteristics in ECMM process with hole within the aspect ratio 0.8 micron meters. The experimental results indicated that the multi-response characteristics considered in electrochemical micromachining of SS304 alloy are enhanced using TOPSIS optimization methodology. ANOVA is used to analyze the process parameters and to identify the best contributing factor in chosen limited parameters. The results indicated that voltage is the most influencing factor which contributes 52.29%. The research possibilities of using PGE electrode are discovered for electrochemical micromachining.

Keywords Electrochemical micromachining · Polymer graphite electrode · TOPSIS · Multi-response optimization

Abbreviations

ECMM	Electrochemical micromachining
PGE	Polymer graphite electrode
V	Voltage (V)
Dc	Duty-cycle (%)
Ec	Electrolytic concentration (g/l)
MRR	Material removal rate (g/min)
Oc	Over-cut (mm)
Ta	Taper angle (degree)

1 Introduction

Considering the industrial change globally, the twenty-first century demands to introduce micro-parts, micro-bots, micro-devices and micro-instruments colossally with feature size in the range of micro-meters. Production of micro-holes is always a challenge. Application of micro-holes with high aspect ratio is extended beyond horizon, such as components like multi-nozzle print heads used in 3D printing, micro-heat vents used in electronic mount technologies, fuel injector nozzle used in automobiles and medical implants in medical industry. The trend in need for miniaturized devices goes with strategic non-traditional manufacturing processes like micro-electro discharge machining, micro-laser beam machining, etc., based on the working principle and for the type of application [1]. This growth explains us that the micromachining technology has boomed up in the chamber of fabricating scale downed products or components, tools for MEMS application. Electrochemical micromachining (ECMM) process is one among the micro-manufacturing technologies that researchers adore to explore because of its benefits like producing stress-free components with high forming accuracy irrespective of the mechanical properties

Technical Editor: Lincoln Cardoso Brandao.

✉ N. Pradeep
natarajanpradeep11@gmail.com

[1] Department of Mechanical Engineering, College of Engineering Guindy Campus, Anna University, Chennai, Tamil Nadu, India

of the material with good surface quality with respect to its finish, ease to machine intricate structures in metallic, ceramic and even the super conductors irrespective of their hardness, heat resistivity and high strength. Compared to electro-discharge micromachining (EDMM) process, it is been observed that ECMM machined parts are subjected to lower thermal stress, no tool wear, higher MRR and with no recast layers, residual stress on the machined surface [1, 2]. It is well known that when compared to laser beam micromachining (LBM), ECMM produces trifling thermal stress after machining, and when compared to abrasive water jet machining AWJMM, ECMM results in restricted erosion with less input energy. This acmes the importance of hole making by ECMM process.

Most of the industries are on track seeing the pros of electrochemical machining and its wide use in processing the materials that are utilized in outrageous states of temperature, corrosion rate, friction factor, etc., and the trend is increasing as evolution occurs [3–5]. This micromachining technology has distinct advantages such as high material removal rate (MRR), good precision and control, diminutive machining time, consistency and flexible multi-process attributes which can be enhanced by coating the micro-tools, using composite electrolytes, introducing additives, and furthermore, it is capable of machining chemically resistant materials and those extensively used in biomedical, electronic and other micromechanical machining applications [6, 7]. The influence on MRR, Ta and Oc was studied using multi-criteria decision-making methodology (MCDM) and ANOVA. The advantages of using PGE remain unexplored in the area of "electrochemical micromachining." An effort has been made to investigate the ECMM process by varying the voltage (V), electrolytic concentration (Ec), duty cycle (Dc) and the output parameters such as MRR, Oc and Ta that are considered together as a multi-objective problem while machining SS304 using PGE as electrode.

2 Electrochemical micromachining system

2.1 Experimental setup

The experimental setup is shown in Fig. 1. Electrochemical micromachining (ECMM) set-up (TTECM-10, Synergy Nano systems, India) and its subcomponents comprise of machining unit, DC pulsed power supply capacity of 20 V, controller unit, jog, tool holder, electrolyte tank, pump. The tool feed is controlled by the stepper motor having a resolution of 0.1 µm per step in *Z*-axis direction. To spot the positions of the workpiece and the tool in the course of machining, transparent acrylic material is used as electrolyte chamber.

2.2 Electrolyte

The electrolytes transfer ions along the tool and workpiece when potential is applied, it eradicates the reaction products, and it also acts as a coolant by eliminating the heat produced due to current flow. Mixed electrolyte with concentration of 1.0 mol/L and 0.01 mol/L of $NaNO_3$ and sodium citrate are used for machining SS304 to increase its MRR by 35% [8, 9]. Stainless steel 304 is known for its high corrosion resistance and for its exceptional machinability. Currently, there is a rise in necessity to machine micro-holes, micro-channels and micro-grooves to precise scale for various applications [8, 10].

In this experiment, priority is given to better machining precision for which sodium nitrate ($NaNO_3$) of varying

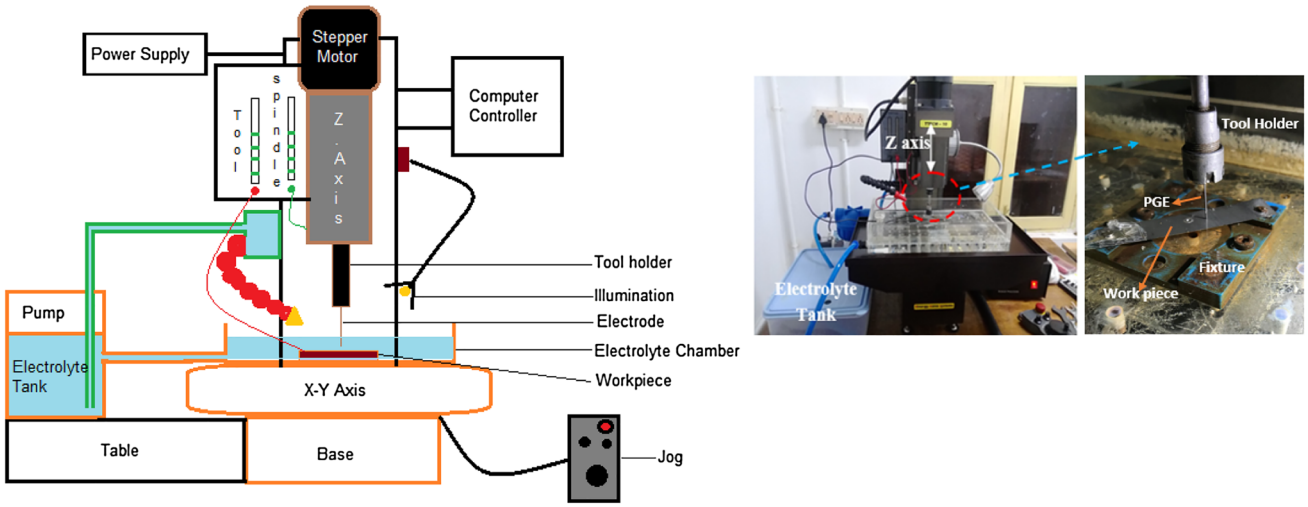

Fig. 1 ECMM experimental setup

concentration is chosen as the electrolyte. $NaNO_3$, which is a passive electrolyte, has the ability to evolve as oxygen forming oxide films in the stray current region. The electrolyte concentration was varied as 23 g, 26 g and 29 g of $NaNO_3$ dissolved in a liter of distilled water. It was observed that MRR increases with increase in concentration of the electrolyte.

2.3 Electrode

In general, electrodes are chosen based on electrical conductivity and electron affinity, materials like copper, brass, tungsten carbide, platinum are widely used, and among those polymer graphite electrodes (PGE), a carbon-based electrode is logically utilized as electrode material in electrochemical applications. Pencil leads are easily available, low cost and disposable, and it exists in two forms—thinner pencil leads with different diameters and thicker diameter wood bound pencil leads. Micro-pencil leads exist in the range of 0.3 mm, 0.5 mm, 0.7 mm and 0.9 mm in diameters. Considering each of the conditions, 0.5 mm diameter is chosen as the tool because of its elastic non-ceramic bonding and resilience with high-temperature carbonized graphite-blended polymer in oxygen-free atmosphere. In wood bound pencil leads, procuring diameter less than 1 mm is challenging due to the availability and poor mechanical characteristics of clay-graphite composition [11]. Chosen pencil leads are non-poisonous and harmless when consumed and also leaves lesser footprint on ecosystem when compared to other electrode materials.

A successful attempt has been made using PGE as electrode material which is of 0.5 mm diameter, a single-use low-cost electrode having comparatively good electrical conductivity among another standard available microelectrode material. EDX is used to know the compositional analysis of polymer graphite presented in Table 1.

2.4 Workpiece material

SS304 workpiece of 400 µm thickness has been selected due to its widespread applications in the areas of automobile, aerospace and in the production of medical equipments like needles, implants for drug delivery, where holes are preferred to be precise and accurate. The composition of SS304 is presented in Table 1.

2.5 Process parameters

Based on the pilot study input parameters, their levels were chosen: voltage (V) in volts, electrolytic concentration (Ec) in g/l and the duty cycle (Dc) in % that govern the ECMM process. The parameters V and Ec are obtained directly, while the parameter Dc is calculated based on the ratio of pulse width time and the total time, i.e., duty cycle is the ratio of pulse on time (µs) to that of total time, where total time is pulse on time plus the pulse off time (µs). Thus, for Dc of 55%, the ratio of pulse on time/pulse off time is 25:20 (µs), and similarly, for Dc of 60% and 65%, the pulse on time/pulse off time is 30:20 (µs) and 37:20 (µs), respectively. Tables 2 and 3 represent the factors and levels that are chosen by adopting Taguchi's design of experiments L27 orthogonal array, which ensures each factor interaction with the input responses, as single variable response. It provides independent relationship with each of the output responses in total. The output responses obtained experimentally during machining are considered to be in the independent directions of vector space. This ensures a complete unique relation with the input parameters during the machining highlighting the significance.

3 Optimization steps using TOPSIS approach

Multi-Response Optimization—Technique for Order of Preference by Similarity to Ideal Solution (TOPSIS) method, is known for its advantages like uncomplicatedness, rationality, clarity, better computational efficiency

Table 2 Process parameters

Symbol	Process parameters	Unit	1st level	2nd level	3rd level
A	Voltage	V	5	7	9
B	Electrolyte concentration	g/l	23	26	29
C	Duty cycle	%	55	60	65

Table 1 Composition of workpiece and electrode material

Stainless steel 304	Ni	Cr	Fe	Si	Mn
Weight%	8.85	16.61	71.71	1.03	1.80
PGE	C	O	Mg	Al	Si
Weight%	71.92	21.08	1.51	3.36	2.13

Table 3 L27 orthogonal array

Experiment no.	Voltage (V)	Electrolyte concentration (g/l)	Duty cycle (%)
1	5	23	55
2	5	23	60
3	5	23	65
4	5	26	55
5	5	26	60
6	5	26	65
7	5	29	55
8	5	29	60
9	5	29	65
10	7	23	55
11	7	23	60
12	7	23	65
13	7	26	55
14	7	26	60
15	7	26	65
16	7	29	55
17	7	29	60
18	7	29	65
19	9	23	55
20	9	23	60
21	9	23	65
22	9	26	55
23	9	26	60
24	9	26	65
25	9	29	55
26	9	29	60
27	9	29	65

and capacity to gauge the relative execution for every alternate option in a basic numerical frame.

3.1 TOPSIS

Parameter responses from least to the most significant are categorized based on the importance of the output responses by decision-maker, such as MRR, Oc and Ta. The details and steps of the Simos' technique were noticed by Ozcan, Figueira and Roy [12]. TOPSIS is a well-known significant tool among researchers for the decision-makers to investigate real-time problems and robustness to give accurate result production than other weighted computational methods [13–15].

By using Simos' technique of weighting criteria, the important individual input weights of the output responses are determined.

Output responses have been arranged, giving priority from the least to the most important, such as MRR, Oc and Ta.

The optimization takes place at four stage levels, using the following procedure [16–18].

Stage 1 Normalized value (unit less) is obtained by excluding the units of all output responses.

Table 4 illustrates the normalized performance matrix (r_{ij}).

Where, x_{ij} = normalized value of ith experimental run associated with the jth output response; i = number of experimental runs; j = number of output responses.

Stage 2 Product of the normalized value with weighted values gives the weighted normalized matrix.

Stage 3 Best alternative performance (Pa+) and worst alternative performance (Pa−) were recognized as every single response in an ideal alternative.

MRR higher, Overcut (less), TA (less).

If jth criteria have a better and worst performance, D+ values and D− values were determined as:

Table 4 Normalized values

Exp. no.	A	B	C	Normalized value		
				MRR	Overcut	Taper angle
1	5	23	55	0.110825	0.125500	0.020169
2	5	23	60	0.157247	0.194926	0.020169
3	5	23	65	0.112110	0.256341	0.201690
4	5	26	55	0.112568	0.226079	0.181549
5	5	26	60	0.168256	0.226079	0.060507
6	5	26	65	0.168073	0.248776	0.221887
7	5	29	55	0.168807	0.175789	0.141211
8	5	29	60	0.168532	0.155318	0.040338
9	5	29	65	0.104495	0.255006	0.464225
10	7	23	55	0.167981	0.196261	0.161380
11	7	23	60	0.166238	0.186470	0.100845
12	7	23	65	0.224678	0.244325	0.060507
13	7	26	55	0.223853	0.185135	0.403380
14	7	26	60	0.224403	0.265245	0.100845
15	7	26	65	0.168256	0.243435	0.141211
16	7	29	55	0.223761	0.198486	0.121042
17	7	29	60	0.223853	0.202492	0.242056
18	7	29	65	0.224587	0.264352	0.060507
19	9	23	55	0.176880	0.065420	0.060507
20	9	23	60	0.212660	0.171339	0.282394
21	9	23	65	0.224403	0.118380	0.121042
22	9	26	55	0.223853	0.094793	0.242056
23	9	26	60	0.224128	0.190921	0.121042
24	9	26	65	0.224036	0.179795	0.141211
25	9	29	55	0.223577	0.091677	0.262225
26	9	29	60	0.224403	0.114819	0.020169
27	9	29	65	0.224036	0.052514	0.262225

Table 5 Closeness coefficient

Exp. no.	D_{ij}^{+}	D_{ij}^{-}	Closeness coefficient	Rank
1	0.036483	0.079645	0.6858	5
2	0.073943	0.036980	0.3333	24
3	0.084140	0.051614	0.3802	21
4	0.080890	0.036092	0.3085	25
5	0.075315	0.053311	0.4144	18
6	0.082454	0.048837	0.3719	22
7	0.070121	0.043617	0.3834	20
8	0.055280	0.076950	0.5819	8
9	0.089954	0.030580	0.2537	27
10	0.058937	0.055177	0.4835	12
11	0.053026	0.064440	0.5485	11
12	0.079454	0.061036	0.4344	15
13	0.084875	0.029557	0.2582	26
14	0.086320	0.054548	0.3872	19
15	0.072752	0.052917	0.4210	16
16	0.067688	0.056568	0.4552	14
17	0.074889	0.039964	0.3479	23
18	0.085443	0.060596	0.4149	17
19	0.005050	0.104494	0.9538	1
20	0.045551	0.077935	0.6311	7
21	0.035776	0.075826	0.6794	6
22	0.028512	0.083072	0.7444	2
23	0.053677	0.068835	0.5618	10
24	0.058268	0.051113	0.4672	13
25	0.032003	0.080157	0.7146	4
26	0.031417	0.084884	0.7298	3
27	0.066644	0.085516	0.5620	9

Pa+: Positive ideal solution; Pa−: Negative ideal solution; Pa+ = [0.02851, 0.03657, 0.01838]; Pa− = [0.03070, 0.07863, 0.09283].

Stage 4 From the Pa+ values, the best alternative distance (Da + ij) and from the Pa− values worst alternative distance of the output responses are kept as (Da − ij).

Table 5 shows the best and worst attributed conditions of each alternatives based on the performance.

Where $i = 1, 2, 3, \ldots, 27$.

Closeness coefficient (Ci) values are determined for each and every alternative. The best alternative is selected conferring to the first choice rank by the order value of Ci, which is accurately nearer to ideal solution, represented as a graph in Fig. 2.

3.2 ANOVA

ANOVA is carried out with a 95% level of confidence and a 5% significant level. It was observed from Table 6 that voltage stood as the most significant process parameter having the *P* value of 0.002 contributing 52.29% resulting in minimum overcut (OC), TA and higher MRR. Among other interactional factors, the III level interaction factor, i.e., the interaction of three factors (V, Ec & Dc) is found to be most influential of the lot that contributing 13.05% and is illustrated using a doughnut chart depicted in Fig. 3. Since all the interactions have been introduced in ANOVA, the *R*-squared value was found to be 100% which indicates that this ANOVA model explains all the variability of the response data around its mean.

Table 7 and the plots in Figs. 4 and 5 highlight the mean response calculated for the closeness coefficient and the interaction between the closeness coefficient, respectively. The process parametric setting A3B1C1 for the ECMM process is the optimal parametric setting.

4 Results and discussion

4.1 Influence of input parameters on MRR

From Fig. 6, it is been inferred that material removal rate is maximum when electrolyte concentration is 29 g and it is minimum at the lower range of electrolyte concentration of 23 g. This is because of the increase in electrical conductivity that occurs due to the low resistance to the current flow, and thus the material removal rate increases when the electrolyte concentration increases. MRR is increased at the voltage of 9 V than that of the lower voltage of 5 V. The material removal rate is high for most of the experiments when the duty cycle is 65%, and the material removal rate is low for most of the experiments when the duty cycle is 55%. MRR increases when the pulse on time increases due to stray current effect which causes high dissolution rate. When the inter-electrode gap decreases, the conductive path length decreases which increases the magnitude of the current and thus the MRR increases as a result of increase in current density. MRR can be controlled by tuning the feed rate.

4.2 Influence of input parameters on overcut

From the experimental plot as shown in Fig. 7, it is found that overcut is maximum at the higher range of electrolyte concentration of 26 g and 29 g. Overcut increases when the voltage increases. It is found that overcut is minimum at a lower voltage of 5 V. As the voltage increases, the overcut also shows a growing trend causing more stray current flow in the machining area forming lesser localization effect, hence resulting in increased overcut. Thus, at the higher range of voltage 9 V and higher range of duty cycle 65% that is a higher pulse on time, the overcut is maximum.

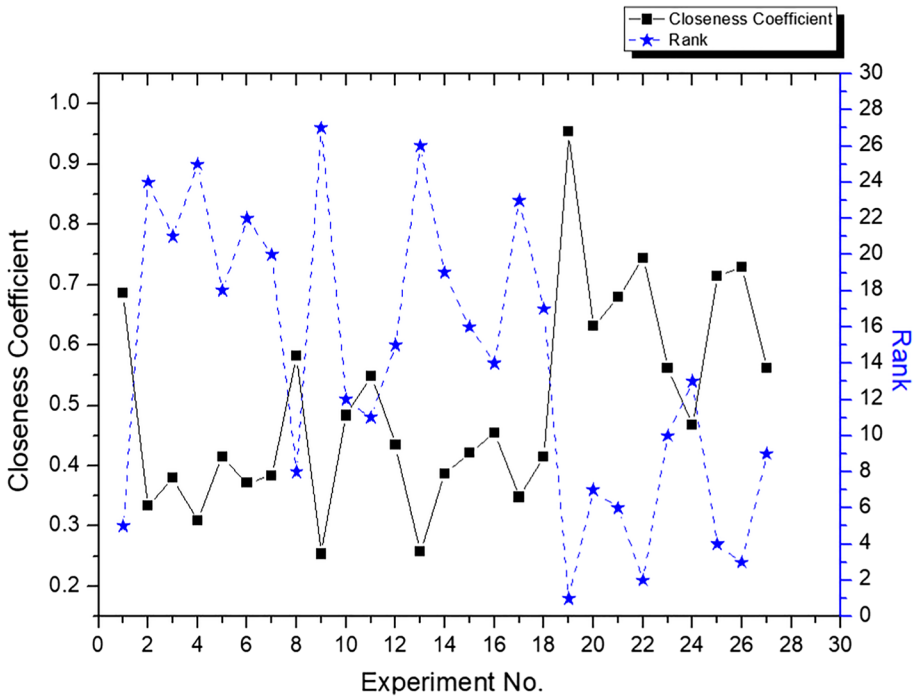

Fig. 2 Closeness coefficient

Table 6 Analysis of variance

Sources	*df*	Sum of square	Mean square	*F* test	*P* value	Contribution %
V	2	0.39608	0.19804	*	*	52.29
Ec	2	0.07997	0.03998	*	*	10.50
Dc	2	0.05604	0.02802	*	*	7.40
V * Ec	4	0.00304	0.00076	*	*	0.40
V * Dc	4	0.05956	0.01490	*	*	7.86
Ec * Dc	4	0.06440	0.01610	*	*	8.50
V * Ec * Dc	8	0.098318	0.012290	*	*	13.05
Error	0	*	*			
Total	26	0.75741				100

*Values less than zero

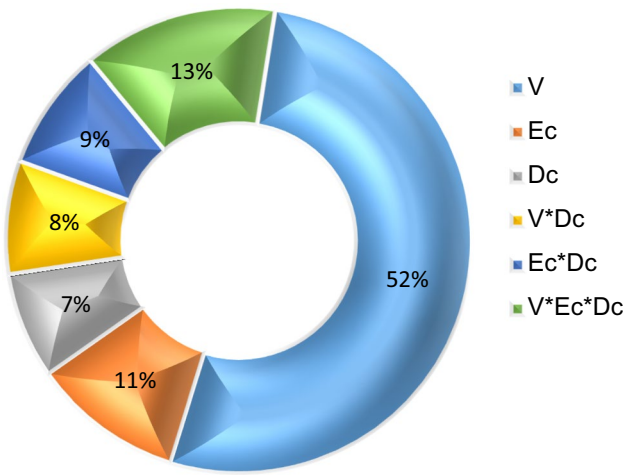

Fig. 3 Contribution of parameters

Table 7 Mean response table

Symbol	A	B	C
Level 1	0.4126	0.5700	0.5542
Level 2	0.4168	0.4372	0.5040
Level 3	0.6716	0.4938	0.4428

4.3 Influence of input parameters on taper angle

From the experimental plot as shown in Fig. 8, it is found that the taper angle is higher when electrolyte concentration is in the high side in the range of 29 g. This phenomenon can be explained by Ohm's law that increases in IEG decreases the side erosion rate. Joule heat is generated at higher machining voltage that causes varying electrolyte

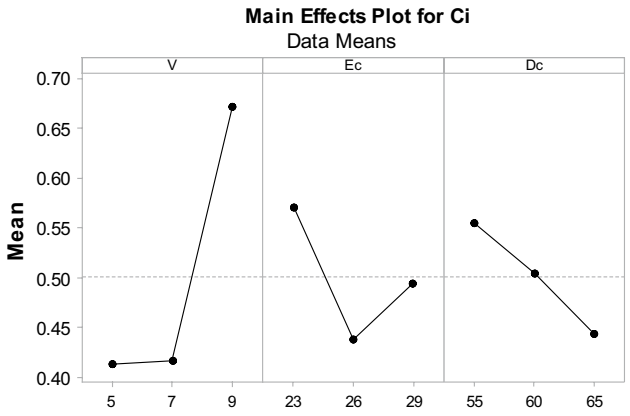

Fig. 4 Mean response plot for the closeness coefficient

conductivity at the IEG forming a non-uniform current distribution which may be the cause for inaccuracy in shape of the work at machined area. It is found that the taper angle is maximum when the duty cycle is at a higher level of 65%, which is due to the higher pulse duration. Increase in pulse duration advances the dissolution in both linear and lateral direction resulting in more material removal in the workpiece causing more side gap.

4.4 Surface morphology study on hole profile of SS304

The lowermost and the uppermost closeness coefficient corresponding to the machined micro-hole are examined using SEM image as depicted in Figs. 9 and 10. The experiment close to the ideal solution obtained from TOPSIS is examined and depicted in the SEM image in Fig. 9 where the precise micro-hole is achieved at 9 V and having 23 g/l of Ec and Dc of 55%, and the experiment farthest from the most ideal solution is shown as SEM image in Fig. 10 where the micro-hole is achieved at the 5 V and having 29 g/l of Ec and a Dc of 65%.

The optimal parameter is found in the experimental data and has a micro-hole of better quality that falls within the aspect ratio having the entry hole side dia of 0.547 mm and exit hole side dia of 0.548 mm, whereas the least preferred parametric setting shows the severe erosion taken up by the work piece when observed at the edges of holes and has the

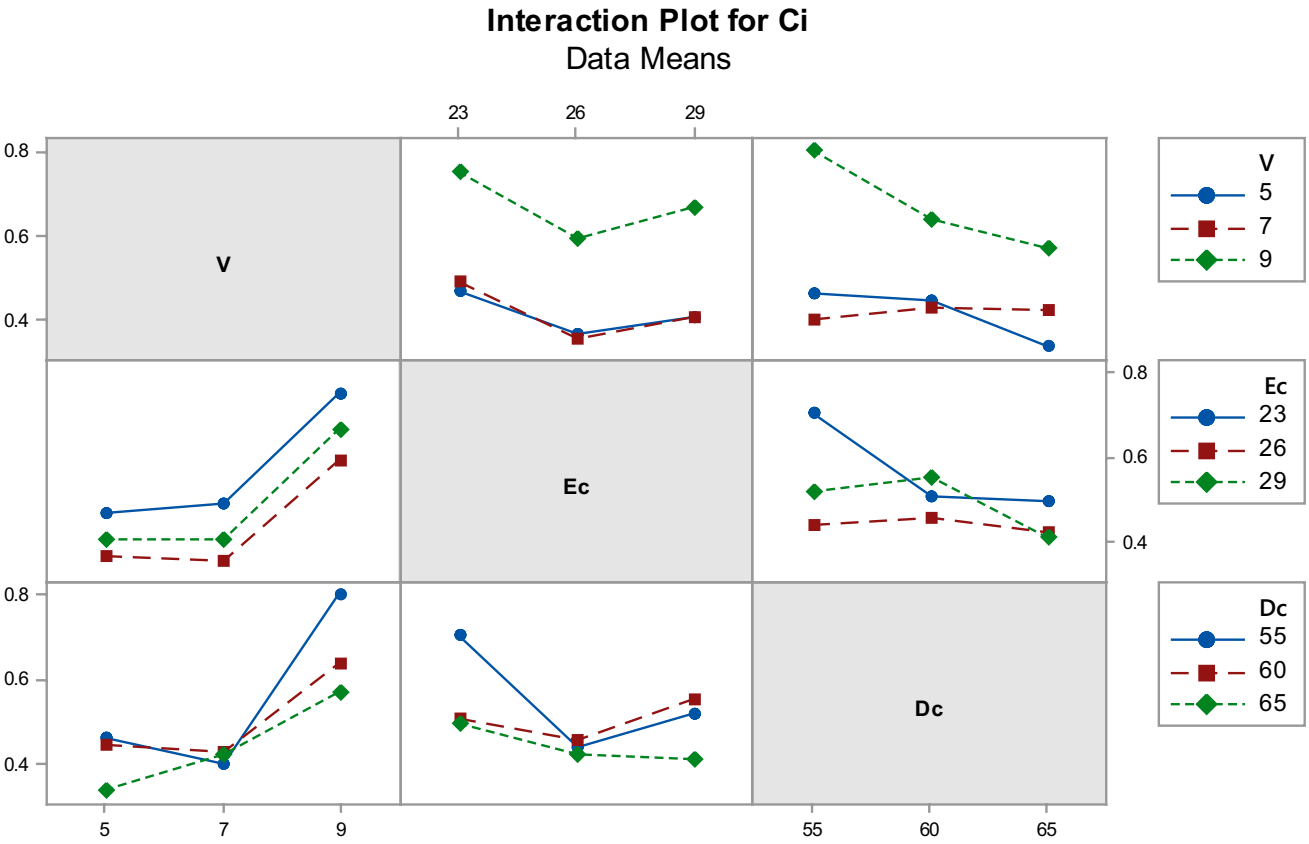

Fig. 5 Interaction plot for the closeness coefficient

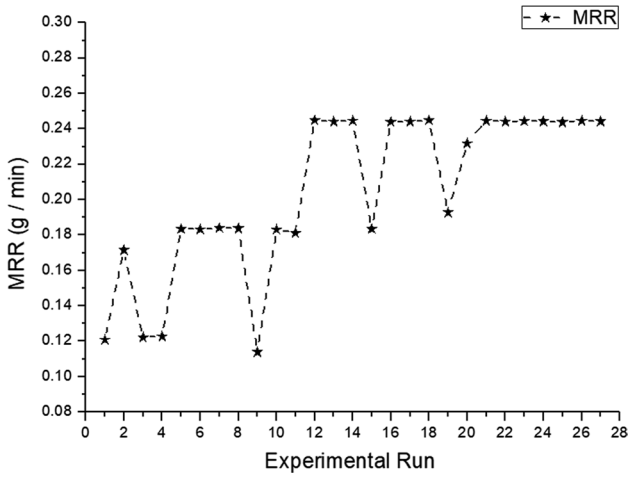

Fig. 6 Influence of V, Ec and Dc on MRR

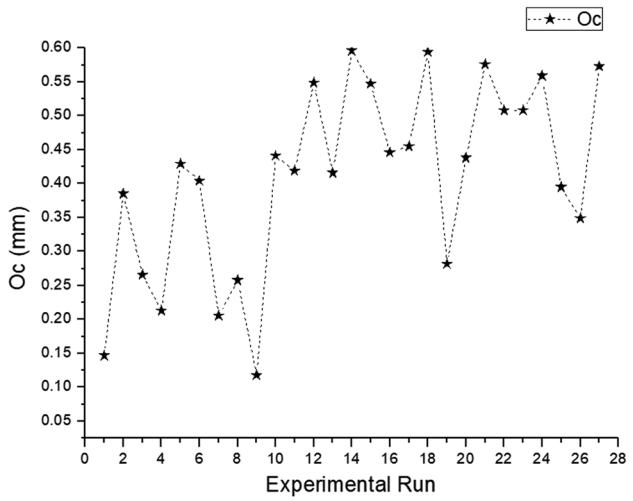

Fig. 7 Influence of V, Ec and Dc on overcut

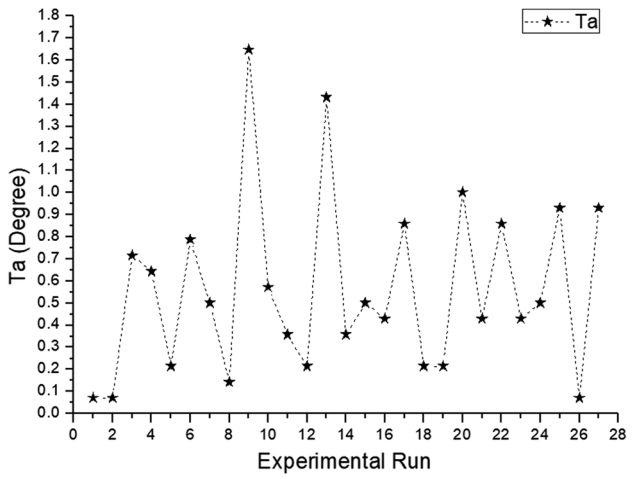

Fig. 8 Influence of V, Ec and Dc on taper angle

poor aspect ratio having the entry hole side dia as 0.973 mm and the exit hole side dia as 0.960 mm having surface irregularities and poor profile of the hole.

From Figs. 9 and 10, it is also seen that the precipitation is observed near the hole edges. The anodic dissolution creates sludges that persists in electrolyte. The liberated hydrogen and oxygen in and around the tool produce gas bubbles and get accumulated on the surface of the electrodes. Controlled pattern of material removal and the shape accuracy of hole in the workpiece get affected particularly by this phenomenon of electrolyte that gets altered by the electrical properties in the machining gap.

It also confirmed that the stray current phenomenon was predominant in micro-hole machined at 5 V. Stray current induced at higher voltages also increases the taper. Even though the lowermost attributed micro-hole has fewer burrs, the overcut is found to be maximum which is shown in Fig. 10 than in the best attributed micro-hole produced. The side wall surface of the machined hole of the lowermost and the best attributed micro-hole is also extracted from Figs. 9 and 10 Side walls with surface irregularity might have caused because of the Joules heat leading to non-uniform current distribution.

5 Conclusions

A detailed investigation through experimental procedure is carried out and clearly studied the influence of electrochemical micromachining process parameters of SS304 alloy using polymer graphite electrode with $NaNO_3$ electrolyte using TOPSIS method. PGE was successfully used as electrode tool, and the optimized process parameter in ECMM was found from the TOPSIS method with the orthogonal array for its multi-response characteristics. The output responses parameters were ranked by using Simos' weighting criteria. The following highlights are listed below:

(1) Material removal rate was maximum at 7 V, with an electrolyte concentration of 23 g and duty cycle of 65%.
(2) Overcut was maximum at voltage of 7 V, with an electrolyte concentration of 26 g and duty cycle of 60%.
(3) Taper angle was maximum at voltage of 5 V, with an electrolyte concentration of 29 g and duty cycle of 65%.
(4) The optimal parametric combination obtained by optimization using the TOPSIS method is 9 V, electrolyte concentration 23 g and duty cycle 55%. The corresponding output response was material removal rate 0.1928 g/min, overcut 0.282 mm and taper angle 0.2148 deg.
(5) The mean response shows that A3B1C1 is the optimal process parametric setting of ECMM process with PGE as a tool.

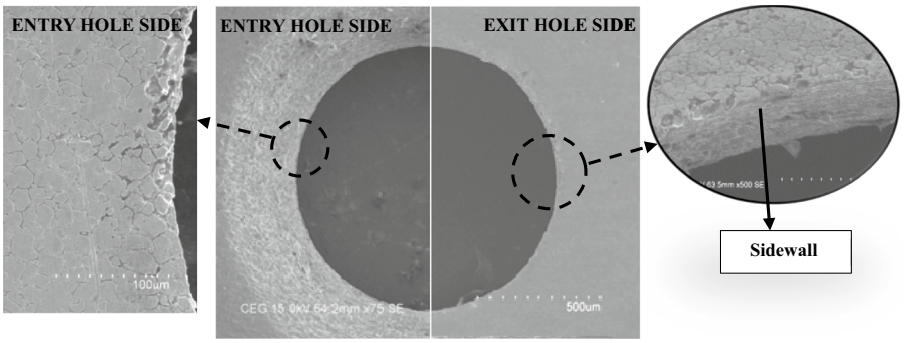

Fig. 9 Micro-hole surface morphology machined at 9 V

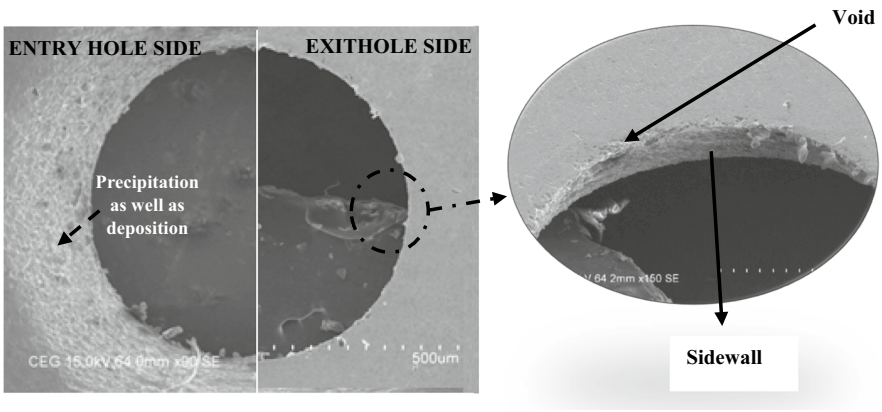

Fig. 10 Micro-hole surface morphology machined at 5 V

(6) Performed ANOVA that identified the contribution of voltage is one of the most significant input parameters which contributes around 52.29% in MRR, Ta and Oc.

Acknowledgements The authors acknowledge the experimental facilities used at the Department of Manufacturing Engineering (DST-FIST) funded, CEG Campus, Anna University.

References

1. Das AK, Kumar P, Sethi A et al (2016) Influence of process parameters on the surface integrity of micro holes of SS304 obtained by micro-EDM. J Braz Soc Mech Sci Eng 38:2029. https://doi.org/10.1007/s40430-016-0488-8
2. Han W, Kunieda M (2019) A novel method to switch machining mode between Micro-ECM and Micro-EDM using oxide film on surface of tungsten electrode. Precis Eng 56:455–465. https://doi.org/10.1016/j.precisioneng.2019.02.002
3. Thanigaivelan R, Arunachalam RM, Karthikeyan B, Loganathan P (2013) Electrochemical micromachining of stainless steel with acidified sodium nitrate electrolyte. Proc CIRP 6:351–355. https://doi.org/10.1016/j.procir.2013.03.011
4. Bhattacharyya B, Munda J, Malapati M (2004) Advancement in electrochemical micro-machining. Int J Mach Tools Manuf 44:1577–1589
5. Pandilov Z (2018) Application of electro chemical machining for materials used in extreme conditions. IOP Conf Ser Mater Sci Eng 329:012014
6. Swain AK (2010) Preparation of coated microtools for electrochemical machining applications. Industrial and Management Systems Engineering—Dissertations and Student Research. Paper 1. http://digitalcommons.unl.edu/imsediss/1
7. Chau OL, Parkan C (1995) Selection of a manufacturing process with multiple attributes—a case study. J Eng Technol Manag 12:219–237
8. Liu G, Yong L, Quancun K, Hao T (2016) Selection and optimization of electrolyte for micro electrochemical machining on stainless steel 304. Proc CIRP 42:412–417. https://doi.org/10.1016/j.procir.2016.02.223
9. Anasane SS, Bhattacharyya B (2016) Experimental investigation on suitability of electrolytes for electrochemical micromachining of titanium. Int J Adv Manuf Technol 86:2147–2160. https://doi.org/10.1007/s00170-015-8309-2
10. Chen C, Li J, Zhan S, Zuyuan Yu, Xu W (2016) Study of microgroove machining by micro-ECM. Proc CIRP 42:418–422. https://doi.org/10.1016/j.procir.2016.02.224
11. Navratil R et al (2016) Polymer lead pencil graphite as electrode material: voltammetric, XPS and Raman study. J Electroanal Chem 783:152–160. https://doi.org/10.1016/j.jelechem.2016.11.030
12. Figueira J, Roy B (2002) Determining the weights of criteria in the ELECTRE type methods with a revised Simos' procedure. Eur J Oper Res 139:317–326. https://doi.org/10.1016/S0377-2217(01)00370-8
13. Durai Prabhakaran RT, Babu BJC, Agrawal VP (2006) Optimum selection of a composite product system using MADM approach. Mater Manuf Process 21(8):883–891. https://doi.org/10.1080/10426910600773472
14. Yuvaraj N, Pradeep Kumar M (2015) Multiresponse optimization of abrasive water jet cutting process parameters using

TOPSIS approach. Mater Manuf Process 30:882–889. https://doi.org/10.1080/10426914.2014.994763
15. Hwang C-L, Yoon K (1981) Multiple attribute decision making. Springer, Berlin. ISBN 978-3-642-48318-9
16. Singh A, Datta S, Mahapatra SS (2011) Application of TOPSIS in the Taguchi method for optimal machining parameter selection. J Manuf Sci Product 11:49–60. https://doi.org/10.1515/jmsp.2011.002
17. Ladeesh VG, Manu R (2018) Machining of fluidic channels on borosilicate glass using grinding-aided electrochemical discharge engraving (G-ECDE) and process optimization. J Braz Soc Mech Sci Eng 40(6):299. https://doi.org/10.1007/s40430-018-1227-0
18. Shakeel Ahmed L, Pradeep Kumar M (2016) Multiresponse optimization of cryogenic drilling on Ti-6Al-4V alloy using topsis method. J Mech Sci Technol 30(4):1835–1841